Analysis of the oscillating photocarrier grating technique



2011 J. Phys. D: Appl. Phys. 44 295103

(http://iopscience.iop.org/0022-3727/44/29/295103)

J. Phys. D: Appl. Phys. **44** (2011) 295103 (12pp) doi:10.1088/0022-3727/44/29/295103

# Analysis of the oscillating photocarrier grating technique

**F Ventosinos**[1,2,4], **N Budini**[1,2], **C Longeaud**[3] **and J A Schmidt**[1,2]

[1] INTEC (UNL-CONICET), Güemes 3450, 3000 Santa Fe, Argentina
[2] FIQ (UNL), Santiago del Estero 2829, 3000 Santa Fe, Argentina
[3] Laboratoire de Génie Electrique de Paris, (UMR 8507 CNRS) Ecole Supérieure d'Electricité, Universités Paris VI et XI, Plateau de Moulon, 91192 Gif-sur-Yvette CEDEX, France

E-mail: fedevento@gmail.com

Received 13 April 2011, in final form 1 June 2011
Published 5 July 2011
Online at stacks.iop.org/JPhysD/44/295103

**Abstract**
In this paper we present a complete theoretical analysis of the oscillating photocarrier grating (OPG) method, starting from the generalized equations that describe charge transport and recombination under oscillating grating illumination conditions. The solution of these equations allows us to implement a calculation reproducing the experimental OPG curves. We study both experimentally and from our calculations the dependence of the OPG curves on different external parameters, such as the applied electric field, grating period and illumination intensity. We find that the response of the sample is linked to a characteristic time of the material, which could be the dielectric relaxation time or the small signal lifetime depending on the regime at which the experiment is performed. Therefore, the OPG technique provides a simple method to estimate these parameters. In addition, we demonstrate that the small signal lifetime provides information on the density of states of the material.

(Some figures in this article are in colour only in the electronic version)

## 1. Introduction

Photocarrier grating techniques are based on making interference between two coherent light beams to form a periodic pattern of light intensity on a sample surface. Areas of high and low light level result in high and low carrier concentrations, respectively. The non-uniform distribution of charges in turn creates an internal electric field, which is affected by the movement of charges by diffusion and drift. When the photocarrier grating is static, the method is called steady-state photocarrier grating (SSPG), and was proposed by Ritter *et al* [1, 2]. This method is now widely used to measure the diffusion length of minority carriers in materials such as hydrogenated amorphous silicon (a-Si : H) [3, 4], microcrystalline silicon [5, 6] and crystalline materials [2, 7]. Moreover, a procedure to extract the density of states (DOS) from SSPG measurements has been proposed [8]. When the photocarrier grating moves with a constant velocity, the method is called the moving grating technique (MGT) and was proposed by Haken *et al* [9, 10]. One of the applications of the MGT was to study electrical transport properties of a-Si : H and its carbon alloys [11]. When the illumination is periodically switched between uniform and with interfringes, the method is known as the modulated photocarrier grating (MPG) technique and was developed by Hattori *et al* [12]. This method has been originally used to test the assumption of ambipolar transport, while a recent analysis of this technique showed that the DOS in the gap of a-Si : H can be estimated from MPG measurements [13]. In this paper we describe another variation of the grating techniques that we call oscillating photocarrier grating (OPG), in which the light grating oscillates with an angular frequency $\omega$.

The grating techniques described so far have been used mainly to characterize amorphous and microcrystalline silicon thin films. However, the same sort of techniques have been previously developed and applied to study photorefractive materials [14–16]. In this field of research, the SSPG technique is known as the 'stationary holographic current' technique, and the MGT as the 'dc photo-electromotive force' (dc photo-EMF) technique. A version of the oscillating grating technique, called 'ac photo-electromotive force', has also been developed at the I F Ioffe Institute in St Petersburg [17].

[4] Author to whom any correspondence should be addressed.

 

Although mainly developed to study photorefractive crystals, this technique has also been sporadically applied to study a-Si : H samples [18–20]. In this dc photo-EMF technique, the amplitude of the oscillations is chosen much smaller than the grating period in order to be able to represent the illumination intensity by a combination of sinusoidal patterns. The variation that we propose here is to use spatial oscillations with amplitude equal to half the grating period, as will be described in the next section. By adjusting the phase shift between both interfering beams, we achieve an oscillation of the interference pattern consisting of a periodic movement with constant velocity in each direction. Therefore, the OPG technique described in this paper can be considered an ac version of the MGT [9] or dc photo-EMF technique [16], allowing for the utilization of synchronous detection and thus reducing the influence of noise. The other difference of our treatment from previous approaches is that we start our theoretical analysis of the method from the DOS of the material, using the multiple trapping model to describe recombination. This way we avoid the use of phenomenological parameters such as the recombination lifetimes introduced in [9] or [16]. Contrary to previous approaches [1, 2, 9, 10, 12] we distinguish between free and trapped charges, achieving a more transparent description of the physics involved. Moreover, we will show that our approach eventually offers the possibility to obtain the DOS of the material from OPG measurements.

This paper is organized as follows. Section 2 presents details about the experiment setup and the preparation of the samples. Section 3 deals with the basic equations that describe the method. Section 4 describes preliminary experimental results obtained from the implementation of this method. In section 5, we discuss our results with the help of numerical calculations that facilitate the interpretation of the physics involved. Finally, section 6 presents the main conclusions of this work.

## 2. Experimental details

The experimental setup used to implement the OPG experiment is presented in figure 1. Two coherent light beams, linearly polarized in the vertical direction, interfere on the sample surface. One of the beams (of intensity $I_2$) goes through an electro-optic modulator (EOM) and impinges perpendicularly to the sample, while the other one (of intensity $I_1$) forms an angle $\delta$ with the other beam. Therefore, an intensity grating with spatial period $\Lambda = \lambda/\sin(\delta)$ is created, where $\lambda$ is the light wavelength (see the appendix). The EOM is positioned so that the axes of the crystal are vertical and horizontal. In this 'phase modulation' configuration, the output amplitude and polarization remain unchanged, but the phase of the wave ($\phi$) is altered as a function of the signal applied to the modulator. The calculation of the resulting illumination intensity $I$ impinging the sample, described in detail in the appendix, gives $I = I_0 + \delta I \cos[kx + \phi(V)]$, where $I_0 = I_1 + I_2$, $\delta I = 2\sqrt{I_1 I_2}$, $V$ is the voltage applied to the EOM and $k = 2\pi/\Lambda$. The phase shift of beam $I_2$ causes the interference pattern to move following the voltage applied to the EOM. In the previously mentioned ac photo-EMF technique [16],

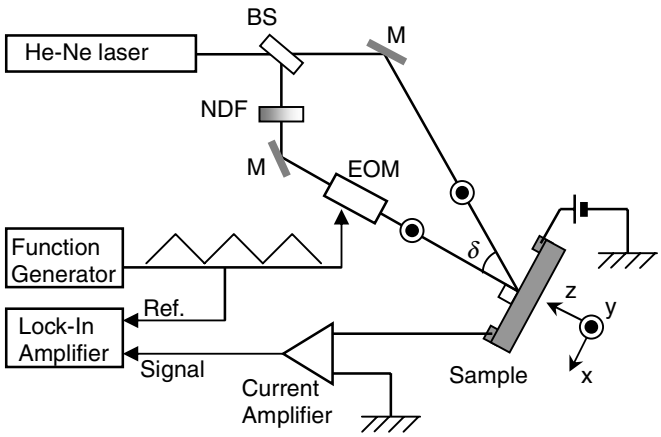


**Figure 1.** Experimental setup for the experiment. A linearly polarized laser beam is split by a beam splitter (BS) into two beams, $I_1$ and $I_2$, which are made to coincide on the sample using the mirrors (M). Beam $I_2$, attenuated by a neutral density filter (NDF), passes through an electro-optic modulator (EOM) used as a phase modulator. These two beams interfere on the sample surface, creating a grating that oscillates depending on the phase shift between both beams. The lock-in amplifier measures the ac photocurrent due to the oscillating grating.

a sinusoidal signal is applied to the EOM giving rise to an illumination intensity $I = I_0 + \delta I \cos[kx - \Delta \sin(\omega t)]$, where $\Delta$ is the amplitude of the oscillation. In that case, the only way to recover a simple sinusoidal expression from this one is to use small modulation amplitudes ($\Delta \ll 1$) [16]. In this paper, we show that information on the sample parameters can also be extracted from an oscillating grating technique even in the case when the amplitude of the oscillations is large. Our proposal is to set $V(t)$ applied to the EOM as a triangular wave function of angular frequency $\omega$ (see the appendix). This gives $I = I_0 + \delta I \cos(kx \pm \omega t)$, where the plus sign is for the first half of the voltage period and the minus sign is for the second half of it. The result is an intensity grating that moves with a constant velocity in one direction for the first half of each period (therefore for half a grating period) and then moves in the opposite direction for the second half of each period. The movement of the intensity grating with a constant velocity in alternate directions makes the OPG technique an ac version of the MGT or dc-photo-EMF technique. The non-uniform illumination leads to a spatially and temporally modulated generation rate, given—for the case of uniform light absorption—by

$$G(x,t) = \frac{\eta I(x,t)(1-R)}{\mathrm{d}\, h\nu}[1 - \mathrm{e}^{-\alpha d}],$$

where $\eta$ is the quantum efficiency of generation of free carriers, $R$ is the reflectance, $d$ is the film thickness, $h\nu$ is the photon energy and $\alpha$ is the absorption coefficient. Therefore, the generation rate can be written as

$$G_{\pm}(x,t) = G_0 + \delta G \cos(kx \pm \omega t) = G_0 + \Re e[\delta G \mathrm{e}^{\mathrm{i}(kx \pm \omega t)}], \quad (1)$$

where $G_0$ and $\delta G$ relate to the homogeneous and modulated part of the illumination $I_0$ and $\delta I$, respectively, $\mathrm{i}^2 = -1$, and $\Re e$ means the real part of the complex number. As will

be shown in the next section this oscillating generation rate results in an alternating current circulating in the direction of the grating movement (for n-type conductivity) [9, 16]. This current is amplified by a low-noise current amplifier with a virtual ground input, thus any voltage drop occurs in the sample. After going through the current amplifier, a lock-in reads this signal as a voltage proportional to the peak value of the first harmonic of the current.

An undoped, 1 $\mu$m-thick a-Si : H sample deposited on a glass substrate was used in the experiments. The deposition was performed by plasma-enhanced chemical vapour deposition from a 3% $SiH_4$/97% Ar gas mixture at a total pressure of 0.3 Torr and a rf power of 2 W. The substrate temperature during deposition was 175 °C. Evaporated Al electrodes were deposited on top of the sample for electrical contacts, disposed in a coplanar geometry with a separation $L_x = 1$ mm between them. The ohmicity of the contacts was verified. The sample was light-soaked for 8 h with a He–Ne laser (632.8 nm, 100 mW cm$^{-2}$) to minimize the effects of light-induced changes in the transport parameters during the experiments. To proceed with the measurements, the intensity relation between the interfering beams was set to $I_2/I_1 \approx 1/20$. Each data point was the result of averaging 90 individual measurements with a delay of 1 s between them.

## 3. Basic equations

To write the basic equations of the technique we shall consider for simplicity a material with monovalent states within the gap, all with the same capture coefficients. The generalization to different species of states having different capture coefficients is straightforward. We will also write the equations for one direction of the running grating; for the other direction we just have to replace $\omega$ by $-\omega$. The spatially and temporally modulated generation rate given by (1) creates distributions of *free* electrons and holes, $n(x,t)$ and $p(x,t)$, with the same period and frequency. However, since electrons and holes have different mobilities and lifetimes, the amplitudes and phases of the two distributions will differ, generating an internal electric field, $\xi_{\text{int}}(x)$. The internal electric field is related to the local charge densities via Poisson's equation

$$\frac{\mathrm{d}\,\xi_{\text{int}}(x,t)}{\mathrm{d}x} = \frac{q}{\varepsilon\varepsilon_0}\left\{ p(x,t) + \int_{E_v}^{E_c} [1 - f(E,x,t)]N^{\text{DON}}(E)\,\mathrm{d}E - n(x,t) - \int_{E_v}^{E_c} f(E,x,t)N^{\text{ACC}}(E)\,\mathrm{d}E \right\}, \tag{2}$$

where $\varepsilon$ is the dielectric constant of the sample, $\varepsilon_0$ is the dielectric permittivity of vacuum, $E_v$ is the energy at the top of the valence band, $E_c$ is the energy at the bottom of the conduction band, $f(E,x,t)$ is the occupation function, $N^{\text{DON}}(E)$ is the density of donor states (neutral when occupied and positively charged when unoccupied) and $N^{\text{ACC}}(E)$ is the density of acceptor states (neutral when empty and negatively charged when occupied). The carrier concentrations $n(x,t)$ and $p(x,t)$ are obtained by solving the continuity equations for electrons and holes, which are

$$\frac{\partial n(x,t)}{\partial t} = G(x,t) - R_n(x,t) + \frac{1}{q}\frac{\partial}{\partial x}[j_n(x,t)], \tag{3}$$

$$\frac{\partial p(x,t)}{\partial t} = G(x,t) - R_p(x,t) - \frac{1}{q}\frac{\partial}{\partial x}[j_p(x,t)], \tag{4}$$

where $q$ is the absolute value of the elementary charge, $R(x,t)$ is the recombination rate and $j(x,t)$ is the current density. Subscripts ($n$ or $p$) refer to electrons or holes, respectively. The recombination rates are given by

$$R_n(x,t) = \int_{E_v}^{E_c} \{c_n n(x,t)[1 - f(E,x,t)] - e_n(E) f(E,x,t)\}N(E)\,\mathrm{d}E, \tag{5}$$

$$R_p(x,t) = \int_{E_v}^{E_c} \{c_p p(x,t) f(E,x,t) - e_p(E)[1 - f(E,x,t)]\}N(E)\,\mathrm{d}E, \tag{6}$$

where $c$ is the capture coefficient, $e(E)$ is the emission rate and $N(E)$ is the DOS. The current densities are the sum of the drift and diffusion components

$$j_n(x,t) = q\mu_n n(x,t)\xi(x,t) + qD_n\frac{\partial n(x,t)}{\partial x} \tag{7}$$

$$j_p(x,t) = q\mu_p p(x,t)\xi(x,t) - qD_p\frac{\partial p(x,t)}{\partial x} \tag{8}$$

where $\mu$ is the extended-state mobility, $D$ is the diffusion coefficient and $\xi(x,t) = \xi_{\text{ext}} + \xi_{\text{int}}(x,t)$ is the total electric field, sum of the externally applied electric field $\xi_{\text{ext}}$ and the internally developed space charge field.

Under the low-modulation condition established when $I_1 \gg I_2$, it is expected that the relevant physical parameters vary sinusoidally as $G(x,t)$ does. In general, however, there will be variable phase shifts, and any quantity $A$ can be expressed as $A(x,t) = A_0 + \Re e[\delta A\, \mathrm{e}^{\mathrm{i}(kx+\omega t)}]$, where $A_0$ is the value under uniform generation rate $G_0$, and $\delta A$ is a complex magnitude originating from the modulated term of the generation rate $\delta G$. Introducing these expressions for $n(x,t)$, $p(x,t)$ and $\xi(x,t)$ into the differential equations (2)–(8) linearizes them, giving rise to the following system of linear complex equations:

$$\begin{cases} \left[\dfrac{1}{\tau_{nn}} + k^2 D_n + \dfrac{(1+Q^-)}{\tau_{\mathrm{d}n}} - \mathrm{i}(\omega + k\mu_n\xi_{\text{ext}})\right] \times \delta n + \left[\dfrac{1}{\tau_{pn}} - \dfrac{(1+Q^+)}{\tau_{\mathrm{d}n}}\right] \times \delta p = \delta G \\ \left[\dfrac{1}{\tau_{np}} - \dfrac{(1+Q^-)}{\tau_{\mathrm{d}p}}\right] \times \delta n + \left[\dfrac{1}{\tau_{pp}} + k^2 D_p + \dfrac{(1+Q^+)}{\tau_{\mathrm{d}p}} - \mathrm{i}(\omega - k\mu_p\xi_{\text{ext}})\right] \times \delta p = \delta G. \end{cases} \tag{9}$$

The coefficients are given by

$$\frac{1}{\tau_{nn}} = c_n \int \left[1 - \frac{(c_n n_0 + e_n)\tau}{1 - \mathrm{i}\omega\tau}\right](1 - f_0)N \,\mathrm{d}E,$$
$$\frac{1}{\tau_{np}} = c_n \int \frac{(c_p p_0 + e_p)\tau}{1 - \mathrm{i}\omega\tau}(1 - f_0)N \,\mathrm{d}E,$$
$$\frac{1}{\tau_{pp}} = c_p \int \left[1 - \frac{(c_p p_0 + e_p)\tau}{1 - \mathrm{i}\omega\tau}\right] f_0 N \,\mathrm{d}E,$$
$$\frac{1}{\tau_{pn}} = c_p \int \frac{(c_n n_0 + e_n)\,\tau}{1 - \mathrm{i}\omega\tau} f_0 N \,\mathrm{d}E,$$
$$Q^- = c_n \int \frac{\tau(1 - f_0)}{1 - \mathrm{i}\omega\tau} N \,\mathrm{d}E,$$
$$Q^+ = c_p \int \frac{\tau f_0}{1 - \mathrm{i}\omega\tau} N \,\mathrm{d}E,$$

$\tau_{\mathrm{d}n} = \varepsilon\varepsilon_0/q\mu_n n_0$ is the electrons' contribution to the dielectric relaxation time, $\tau_{\mathrm{d}p} = \varepsilon\varepsilon_0/q\mu_p p_0$ is the holes' contribution to the dielectric relaxation time. The integrals are evaluated between $E_\mathrm{v}$ and $E_\mathrm{c}$ (the energy dependence is omitted for the sake of clarity), and we call $\tau^{-1} = c_n n_0 + c_p p_0 + e_n + e_p$. The subscript 0 is used to denote quantities under steady-state equilibrium with the generation rate $G_0$.

The total current density flowing through the sample will be given by

$$j(t) = j_n(x,t) + j_p(x,t) + \varepsilon\varepsilon_0 \frac{\partial \xi_{\mathrm{int}}(x,t)}{\partial t}, \tag{10}$$

where the last term is the displacement current (the external electric field is time-independent). If we integrate (10) through the variable $x$ along the interelectrode spacing $L_x$, we obtain

$$L_x j(t) = \int_0^{L_x} [j_n(x,t) + j_p(x,t)]\,\mathrm{d}x + \varepsilon\varepsilon_0 \frac{\partial}{\partial t}\int_0^{L_x} \xi_{\mathrm{int}}(x,t)\,\mathrm{d}x. \tag{11}$$

The last term vanishes when integrated due to the potential nature of the electric field and the periodicity of the quantities [12, 16]. The integrals of the diffusion components of the current densities also vanish due to the periodicity [12, 16]. Therefore, the only contribution to the experimentally measured current comes from the drift component, which is given by

$$j(t) = \frac{1}{\Lambda}\int_0^{\Lambda} [q\mu_n n(x,t) + q\mu_p p(x,t)] \times [\xi_{\mathrm{ext}} + \xi_{\mathrm{int}}(x,t)]\,\mathrm{d}x = j_0 + \delta j(t), \tag{12}$$

where the integration can be performed over one period of the interference provided the interelectrode spacing is much larger than the grating period [12, 16]. The constant and modulated parts of the current density are given by $j_0 = q(\mu_n n_0 + \mu_p p_0)\xi_{\mathrm{ext}}$ and

$$\delta j(t) = \frac{1}{\Lambda}\int_0^{\Lambda} \left[q\mu_n \delta n(x,t) + q\mu_p \delta p(x,t)\right] \xi_{\mathrm{int}}(x,t)\,\mathrm{d}x = \frac{1}{\Lambda}\int_0^{\Lambda} j_{\mathrm{dr}}(x,t)\,\mathrm{d}x, \tag{13}$$

where $j_{\mathrm{dr}}(x,t)$ is the drift component of the total current density. From the solution of the system (9), analytical expressions for $\delta n(x,t)$ and $\delta p(x,t)$ can be obtained. Inserting them into (13), it is found that $\delta j(t)$ has the following expression:

$$\delta j_{\pm\omega} = \tfrac{1}{2}\Re e(\delta\sigma_\pm \times \delta\xi_\pm^*), \tag{14}$$

where the superscript * means the complex conjugate, $\delta\sigma_\pm = q(\mu_\mathrm{n}\delta n_\pm + \mu_\mathrm{p}\delta p_\pm)$ and $\delta\xi_\pm = (\mathrm{i}q/k\varepsilon\varepsilon_0)[(1 + Q_\pm^-)\delta n_\pm - (1 + Q_\pm^+)\delta p_\pm]$. The only time dependence comes from the periodic change in the direction of circulation of the current. The oscillating intensity grating results in a current density that alternates between two constant values, $\delta j_{+\omega}$ and $\delta j_{-\omega}$, corresponding to the currents created by the grating moving in each direction. This is shown in figure 2 for measured and simulated data for the case of no external electric field. Figure 2(*a*) is a photograph of the screen of an oscilloscope that registers a signal proportional to $\delta j(t)$. To visualize this signal with the oscilloscope we had to amplify it quite a lot, giving rise to bandwidth limitations. The signal of figure 2(*a*), having a frequency of 2 kHz, was recorded with a gain of $10^9$and a bandwidth of 7 kHz. Despite the noise blurring the signal, it can be seen that the shape of the wave is not exactly a square. However, this shape fits with the answer $V_{\mathrm{out}}$ expected from a low pass second-order filter with a bandwidth of 7 kHz to an input square signal $V_{\mathrm{in}}$ of 2 kHz frequency (figure 2(*b*), dashed line). Therefore, we are confident that $\delta j(t)$, the current density created by the oscillating grating, is indeed a square wave function of time (figure 2(*b*), solid line). Considering that the lock-in amplifier measures the first harmonic of this square wave signal, the distortion introduced by the current amplifier should not affect the final reading of this instrument. Therefore, we end up with a current density that we shall call the OPG current density in the following:

$$\delta j_{\mathrm{OPG}} = \frac{\sqrt{2}}{\pi}(\delta j_{+\omega} - \delta j_{-\omega}). \tag{15}$$

## 4. Experimental results

Figure 3 presents the results of two OPG measurements performed on the a-Si : H sample as a function of the external electric field, keeping fixed the grating period ($\Lambda = 8.6\,\mu$m) and the generation rate ($G_0 = 3.9 \times 10^{20}\,\mathrm{cm^{-3}\,s^{-1}}$). The frequency of the signal driving the EOM was varied between 1 and 90 kHz, meaning that the grating velocity varied between 0.86 and 77 cm s$^{-1}$. A well-defined maximum for $\omega \cong 1.7 \times 10^5\,\mathrm{s^{-1}}$ can be appreciated, with a symmetric peak in logarithmic scales. An electric field of 40 V cm$^{-1}$ was applied to the sample in one of the measurements (circles), while the other one (diamonds) was obtained under short-circuit conditions.

As can be seen, both curves are equal within the experimental error, meaning that this relatively low electric field does not alter the current that circulates through the sample. The shape of the curve is similar to those obtained using the MGT (or dc photo-EMF technique), as expected due to the common origin of both techniques.

Figure 4 presents the results of a series of OPG measurements performed as a function of the grating period, keeping fixed the generation rate ($G_0 = 6.0 \times 10^{20}\,\mathrm{cm^{-3}\,s^{-1}}$)

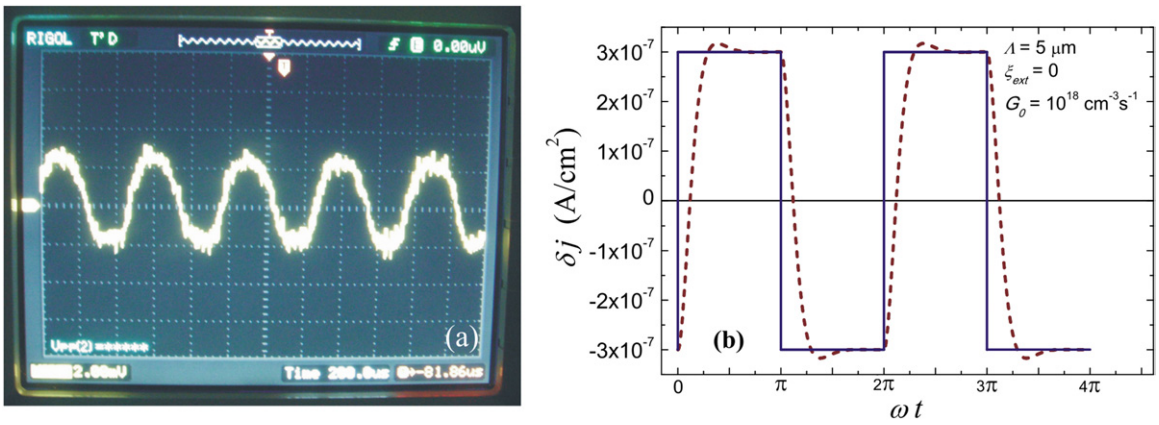


**Figure 2.** Measured (*a*) and simulated (*b*) current density that circulates through the sample as a function of time for a zero external electric field. In (*a*) the square wave is slightly rounded due to the limited bandwidth of the current amplifier. A small external electric field would shift the mean value without changing the amplitude of the signal.

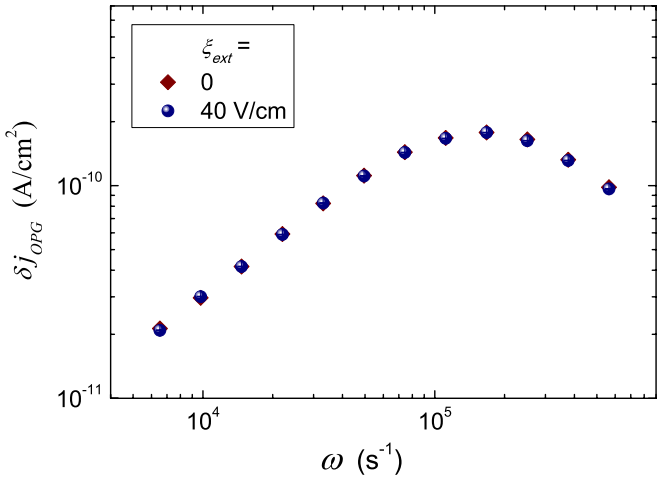


**Figure 3.** OPG current density ($\delta j_{\mathrm{OPG}}$) as a function of the angular frequency ($\omega$) of the signal applied to the EOM, for zero external electric field (diamonds) and for 40 V cm$^{-1}$ (circles).

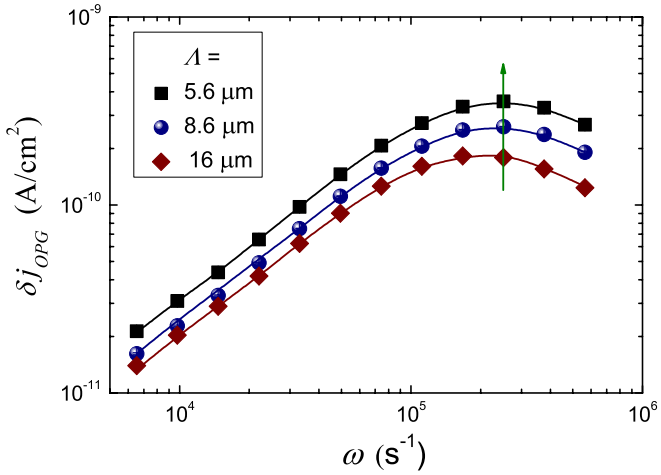


**Figure 4.** OPG current density ($\delta j_{\mathrm{OPG}}$) as a function of the angular frequency ($\omega$) of the signal applied to the EOM, for different values of $\Lambda$ indicated in the figure. The generation rate is fixed at $6.0 \times 10^{20}$ cm$^{-3}$ s$^{-1}$ and the measurements are carried out in a short circuit configuration. The lines and the arrow are guide to the eye.

and the external electric field (short-circuit conditions). As can be seen, the angular frequency that gives the highest value of the current density ($\omega_{\max}$) does not change, but the maximum value increases with a decrease in $\Lambda$. All the curves exhibit the same shape, being only vertically displaced.

Figure 5 presents the results of a series of OPG measurements performed as a function of the generation rate, keeping fixed the grating period ($\Lambda = 20\,\mu$m) and the external electric field (short-circuit conditions). The three curves present the same slope in the low-frequency region, with a linear increase in $\delta j_{\mathrm{OPG}}$ with $\omega$. An increase in the generation rate causes a displacement of $\omega_{\max}$ to higher values. At the same time, an increase in the maximum value of the current density is also observed. These experimental observations will be further explained in the next section.

## 5. Discussion

In this section we shall explain the origin of the OPG signal, and the three main features of our measurements: that a moderate external electric field does not alter the curves, that an increase in the grating period causes a decrease in the signal without changing the position of the maximum, and that an increase in the illumination intensity causes an increase in the signal and a shift of the maximum towards higher frequencies. Finally, we will outline a method based on OPG measurements to obtain the DOS as a function of energy in the upper half of the bandgap.

### *5.1. Illustration by means of numerical modelling*

In order to have access to some quantities that cannot be measured, we have performed a numerical simulation of the experiment. The DOS that we have used, which is quite typical for hydrogenated amorphous silicon, is shown in figure 6. The characteristic slopes for the band tails are 55 meV for the valence tail and 27.5 meV for the conduction tail, while the maximum defect densities are $2 \times 10^{16}$ cm$^{-3}$ eV$^{-1}$ for both donor (Gaussian function centred at 0.85 eV, standard deviation of 0.12 eV) and acceptor (Gaussian function centred at 1.25 eV,

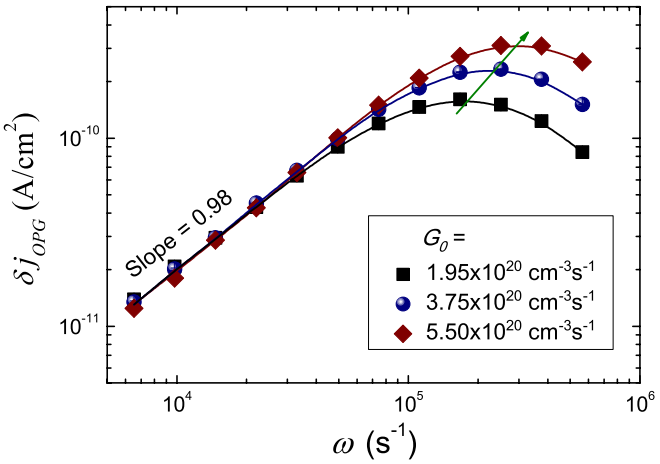


**Figure 5.** OPG current densities ($\delta j_{\mathrm{OPG}}$) obtained for different values of the generation rate indicated in the figure. The grating period was set as $\Lambda = 20\,\mu$m and the measurements were performed in a short-circuit configuration. The lines and the arrow are guide to the eye.

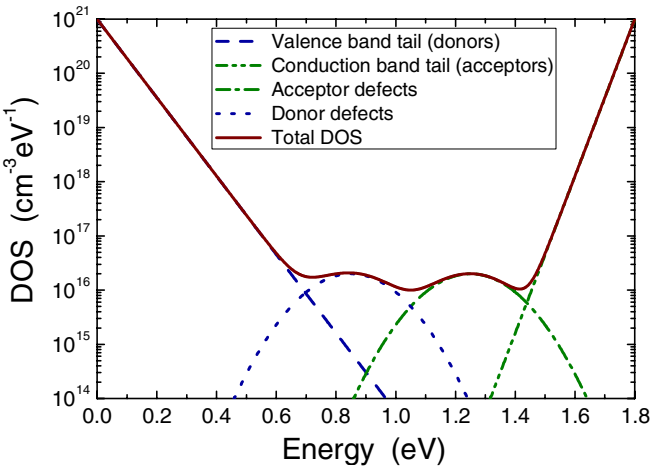


**Figure 6.** Typical DOS for a-Si : H used in our simulations.

standard deviation of 0.12 eV) distributions of states. We have chosen standard values for the material parameters, such as carrier mobilities $\mu_n = 10\,\mathrm{cm^2\,V^{-1}\,s^{-1}}$, $\mu_p = 1\,\mathrm{cm^2\,V^{-1}\,s^{-1}}$ and capture coefficients $c_n = c_p = 4 \times 10^{-9}\,\mathrm{cm^3\,s^{-1}}$.

The system of equations (9) can be analytically solved for each value and each sign of $\omega$. We have developed a computer code that numerically calculates the integrals defining the coefficients of (9), and thus calculates $\delta n$ and $\delta p$. Then, the internal electric field and conductivity are computed and the evolution of the OPG current with $\omega$ is calculated. The purpose of the calculations is not to fit the experimental results, but to follow the evolution of quantities that are not accessible from the experiment. By doing so, we get a better understanding of the physics involved.

We shall first explain the origin of the OPG signal and the general shape of the $\delta j$ versus $\omega$ curves. The grating illumination creates a periodic spatial distribution of free and trapped charge. In figure 7 we present a 'picture' of the distribution inside the sample of different quantities at a given time $t^*$, as obtained from our calculations for the light grating

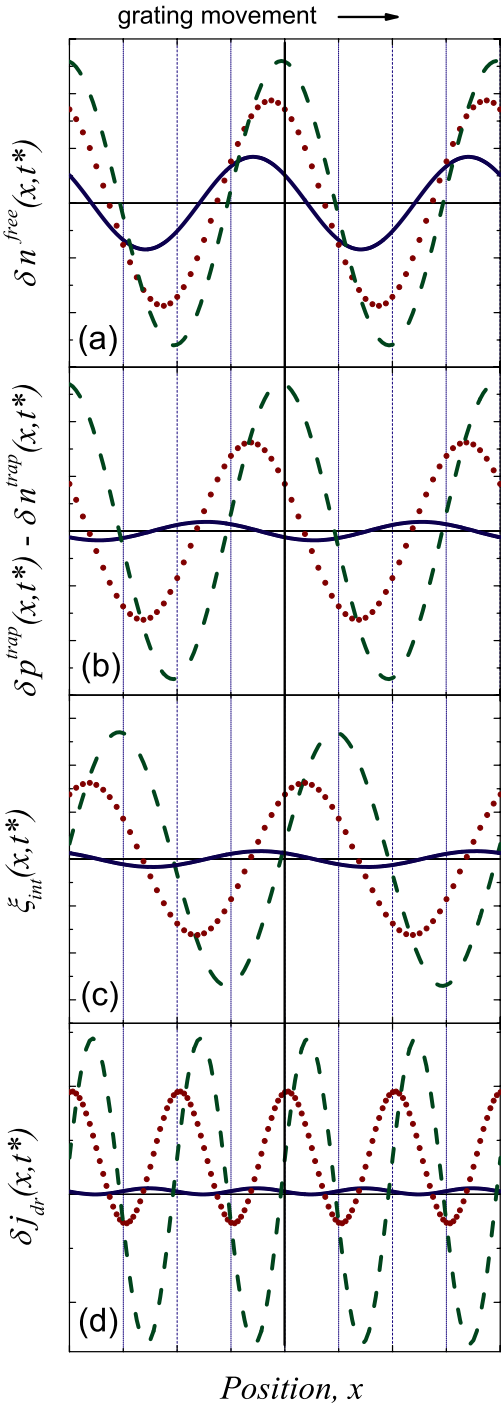


**Figure 7.** Numerical calculations of ($a$) the distributions of free electrons ($\delta n^{\mathrm{free}}(x, t^*)$), ($b$) net trapped charge ($\delta p^{\mathrm{trap}}(x, t^*) - \delta n^{\mathrm{trap}}(x, t^*)$), ($c$) internal electric field ($\xi^{\mathrm{int}}(x, t^*)$) and ($d$) the resulting drift component of the OPG current density ($\delta j_{\mathrm{dr}}(x, t^*)$), as a function of the spatial coordinate $x$ at a given time $t^*$ while the illumination grating moves steadily to the right. The dots correspond to the grating angular frequency that gives the maximum OPG signal, the dashed line to a much lower frequency and the solid line to a much higher frequency (see also figure 8).

moving in the positive $x$ direction. The position of one maximum of the light grating is shown by a vertical solid line. Three different cases, corresponding to three $\omega$ values, are displayed in each figure: the dots correspond to the grating angular frequency that gives the maximum OPG signal, the

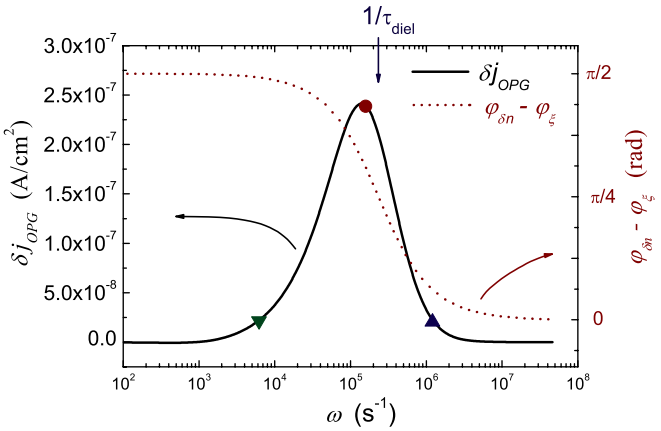


**Figure 8.** Calculated OPG signal ($\delta j_{\mathrm{OPG}}$, left axis) and phase shift between the free electrons and the internal electric field ($\varphi_{\delta n} - \varphi_{\xi}$, right axis) as a function of grating oscillation angular frequency ($\omega$). The symbols correspond to the frequencies used to construct figure 7. The inverse of the dielectric relaxation time is indicated by a vertical arrow.

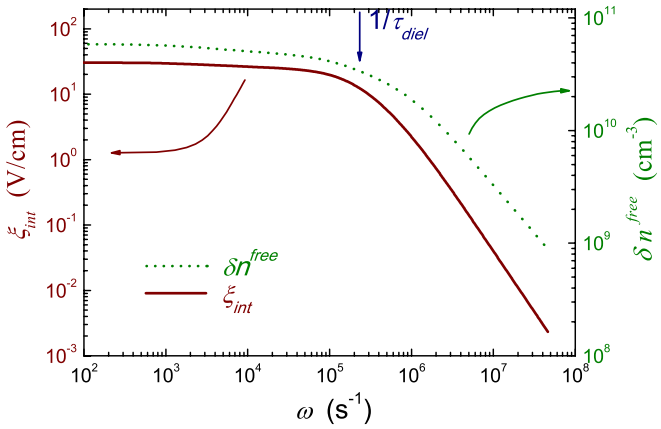


**Figure 9.** Evolution of the values of the internal electric field ($\xi_{\mathrm{int}}$, left axis) and free electrons ($\delta n^{\mathrm{free}}$, right axis) as a function of the angular frequency.

dashed line to a much lower frequency and the solid line to a much higher frequency (these angular frequencies are indicated in figure 8).

The distribution of *free* electrons $\delta n^{\mathrm{free}}(x, t^*)$ created by the modulated illumination $\delta G$ (calculated from (9)) can be seen in figure 7($a$). In the case of intrinsic amorphous silicon the transport is dominated by electrons rather than holes, so the distribution of free electrons will define the resulting current. Figure 7($b$) presents the corresponding plot for the net trapped charge (difference between positive and negative trapped charges $\delta p^{\mathrm{trap}}(x, t^*) - \delta n^{\mathrm{trap}}(x, t^*)$). As can be seen, the curves for the lowest frequency (dashed lines in ($a$) and ($b$)) are almost in phase between them and with the illumination. In a material like a-Si : H, with a large DOS in the band gap, the trapped charge is usually much larger than the free charge. Therefore, figure 7($b$) can be considered a plot of the total excess charge. According to Poisson's equation (2), the inhomogeneous charge density creates an internal electric field even for the case of no external electric field applied to the sample.

A straightforward calculation shows that this internal electric field is 90° out of phase with the space charge, as can be seen in figure 7($c$). The drift component of the current density, $\delta j_{\mathrm{dr}}(x, t^*)$, is presented in figure 7($d$). As shown in section 3, it is the average of $\delta j_{\mathrm{dr}}(x, t)$ over one spatial period that defines the current measured in the OPG experiment. For low frequencies, free charges and the internal electric field are 90° out of phase, and thus the current oscillates around zero (dashed line in figure 7($d$)). A static grating gives a current whose mean value (calculated according to (13)) vanishes, being the reason for the fact that all the OPG current densities tend to zero for $\omega \to 0$.

When the grating oscillation frequency increases, charges start to lay behind the light excitation (dots in figures 7($a$) and ($b$)). However, free charges can respond much faster than trapped charges, and a phase shift between both distributions arises. The internal electric field (dots in figure 7($c$)), which is determined mainly by the trapped charge, starts to be partially in phase with the free charges. As a result, $\delta j_{\mathrm{dr}}(x, t)$ oscillates in space around a nonzero value (dots in figure 7($d$)). When $\delta j_{\mathrm{dr}}(x, t)$ is averaged over one period (equation (13)), the resulting $\delta j(t)$ does not vanish even for zero external electric field. The value of $\delta j(t)$ is constant as long as the grating moves with a constant velocity in one direction ($\delta j_{+\omega}$), and changes sign when the grating changes the direction of movement ($\delta j_{-\omega}$, see figure 2).

For even higher frequencies (solid lines), the phase shift between free and trapped charges increases further. At the same time, the fact that trapped carriers cannot follow the excitation causes a blurring of the charge distributions (see figure 7($b$), solid line). As a result, the internal electric field tends to vanish (figure 7($c$), solid line). Even when the internal electric field turns to be in phase with the distribution of free electrons, therefore $\delta j_{\mathrm{dr}}(x, t)$ being always positive in this case (figure 7($d$), solid line), the steady blurring of the space charge grating leads to a decrease in its amplitude. Consequently, the OPG current tends to vanish for the highest frequencies.

The information presented for a given time $t^*$ as a function of the position inside the samples in figure 7 can be considered differently and presented as the amplitudes and phase shifts of the different quantities, as in figures 8 and 9. In figure 8 we show the evolution of the OPG signal, $\delta j_{\mathrm{OPG}}$, and of the phase shift between free electrons and the internal electric field, $\varphi_{\delta n} - \varphi_{\xi}$, as a function of $\omega$. The points marked by symbols in the figure correspond to the three angular frequencies presented in figure 7. In this calculation we have used a generation rate $G_0 = 10^{18}\,\mathrm{cm^{-3}\,s^{-1}}$, a grating period $\Lambda = 20\,\mu\mathrm{m}$ and an external electric field $\xi_{\mathrm{ext}} = 0$. As can be seen, for low frequencies the phase shift between the internal field $\xi_{\mathrm{int}}$ and the excess of free carriers $\delta n^{\mathrm{free}}$ tends towards $\pi/2$ and $\delta j_{\mathrm{OPG}}$ towards zero, as we have already explained. For high enough frequencies, $\xi_{\mathrm{int}}$ and $\delta n^{\mathrm{free}}$ get to be in phase, but $\delta j_{\mathrm{OPG}}$ tends to zero again. This is because $\xi_{\mathrm{int}}$ and $\delta n^{\mathrm{free}}$ both tend to decrease when the frequency is increased.

Figure 9 presents this behaviour, from where it can be seen that the decrease in $\delta j_{\mathrm{OPG}}$ for angular frequencies larger than $\sim 1.6 \times 10^5\,\mathrm{s^{-1}}$ (marked with a dot in figure 8) is coincident with the sharp decrease in $\xi_{\mathrm{int}}$ and $\delta n^{\mathrm{free}}$ in figure 9.

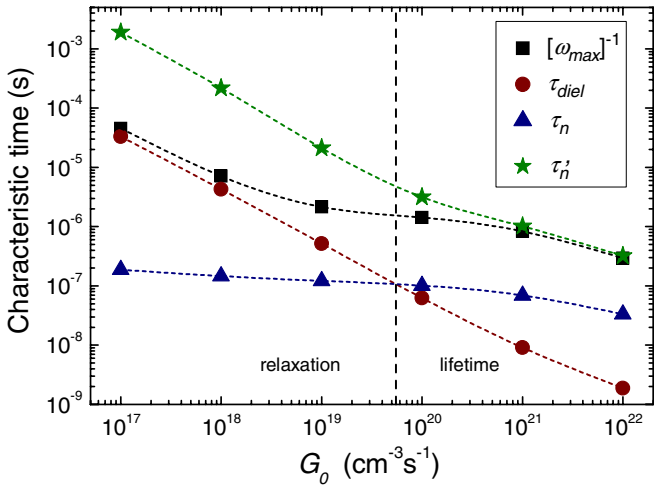


**Figure 10.** Calculated results showing the evolution of different characteristic times with the generation rate.

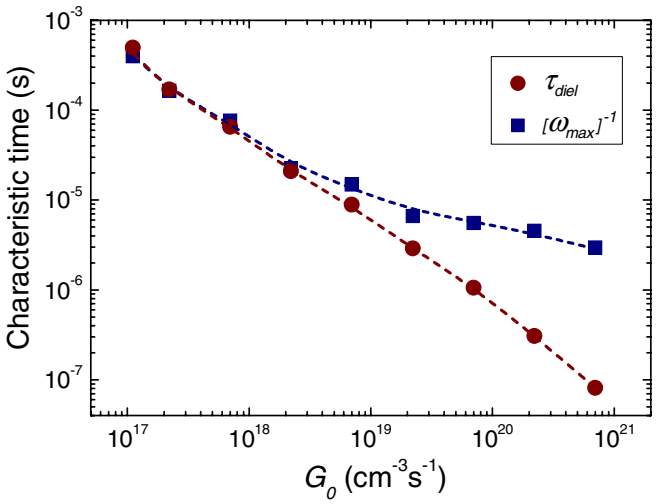


**Figure 11.** Experimental result showing the evolution of the dielectric relaxation time and of $\omega_{\max}^{-1}$ as a function of the generation rate.

Putting both facts together, we can understand the shape of the OPG curves: at low frequencies, free and trapped charges are in phase between them but out of phase with the internal electric field, so there is low OPG signal despite the high values of the charges. When the frequency begins to rise, free and trapped charges begin to be out of phase due to their different response times. The electric field begins to be partially in phase with the free carriers, so the photocurrent increases. This continues until the point when the trapped carriers can no longer follow the movement of the light grating, causing a blurring of the charge grating. From that point on, the photocurrent begins to decrease due to the decrease in both the electric field and electron concentration.

### 5.2. *Characteristic times of the semiconductor*

The angular frequency that gives the maximum OPG signal, $\omega_{\max}$, is clearly related to some characteristic time of the sample, which couples with the oscillation of the grating. The different characteristic times that can be considered are the free electron lifetime $\tau_n$, the dielectric relaxation time $\tau_{\text{diel}}$ and the recombination time of the small excess of free plus trapped electrons, that we shall call the small signal electron lifetime $\tau_n'$ in the following. This small signal electron lifetime is defined as $\tau_n' = (\delta n^{\text{trap}} + \delta n^{\text{free}})/\delta G = \delta n^{\text{tot}}/\delta G$, following the definition given in [21, 22]. The link between these different characteristic times and the inverse of $\omega_{\max}$ is clarified in figure 10, where we present the calculated dependence of $\tau_n$ (triangles), $\tau_n'$ (stars), $\tau_{\text{diel}}$ (circles) and $\omega_{\max}^{-1}$ (squares) as a function of $G_0$. The characteristic times were calculated by numerically solving the continuity and charge neutrality equations in the steady state. As can be seen, for these particular 'material' parameters, a generation rate of $\sim 5 \times 10^{19}\,\text{cm}^{-3}\,\text{s}^{-1}$ defines the limit between the relaxation regime ($\tau_n < \tau_{\text{diel}}$ for $G_0 < 5 \times 10^{19}\,\text{cm}^{-3}\,\text{s}^{-1}$) and the lifetime regime ($\tau_n > \tau_{\text{diel}}$ for $G_0 > 5 \times 10^{19}\,\text{cm}^{-3}\,\text{s}^{-1}$).

In the relaxation regime $\omega_{\max}^{-1}$ tends towards $\tau_{\text{diel}}$, which is easy to understand since this time governs the formation of the space charge field. The inverse of $\tau_{\text{diel}}$ is marked by a vertical arrow in figures 8 and 9, and is roughly coincident with the maximum in the OPG curve and the sharp decrease in $\delta n$ and $\xi_{\text{int}}$. This is expected since the generation rate used in those calculations ($G_0 = 10^{18}\,\text{cm}^{-3}\,\text{s}^{-1}$) locates the sample in the relaxation time regime. Therefore, $\tau_{\text{diel}}$ can be obtained from an OPG measurement performed with a low-enough generation rate. Since $\tau_{\text{diel}}$ can also be obtained from the steady-state photoconductivity ($\sigma_0$) as $\tau_{\text{diel}} = \varepsilon\varepsilon_0/\sigma_0$, we are in a position to verify the results of our calculations. Figure 11 presents the results of measurements performed at different generation rates, where $\tau_{\text{diel}}$ (circles) and $\omega_{\max}^{-1}$ (squares) are displayed as a function of $G_0$. As can be seen, $\omega_{\max}^{-1}$ tends towards $\tau_{\text{diel}}$ in the limit of low generation rates, when the sample is certainly in the relaxation regime.

On the other hand, figure 10 shows that in the lifetime regime $\omega_{\max}^{-1}$ tends to $\tau_n'$. This can be understood since $\tau_n'$ is the characteristic time at which excess trapped charges relax, giving rise to a blurring of the charge grating. Since we are under small signal modulation conditions, the response of the sample to an external perturbation is characterized by the small signal lifetime $\tau_n'$. An OPG measurement performed with a high generation rate would provide $\tau_n'$ from the inverse of $\omega_{\max}$. This is an important result, since it is not easy to obtain $\tau_n'$ in materials exhibiting dispersive transport, such as a-Si : H. Transient methods fail to provide a definite value, since the photocurrent decay is not a single exponential [23, 24]. Therefore, the possibility to obtain $\tau_n'$ from a different experiment is stimulating.

### 5.3. *Interpretation of the experimental results*

We are now in a position to explain the behaviour of the sample in the experimental tests. In figure 12 we plot the OPG current as a function of $\omega$, calculated for the DOS of figure 6 from the equations of section 3, for $G_0 = 10^{21}\,\text{cm}^{-3}\,\text{s}^{-1}$, $\Lambda = 40\,\mu\text{m}$ and for different values of the external electric field. The DOS of figure 6 is not chosen to fit the experimental results; it is just a typical DOS for a-Si : H. For that reason,

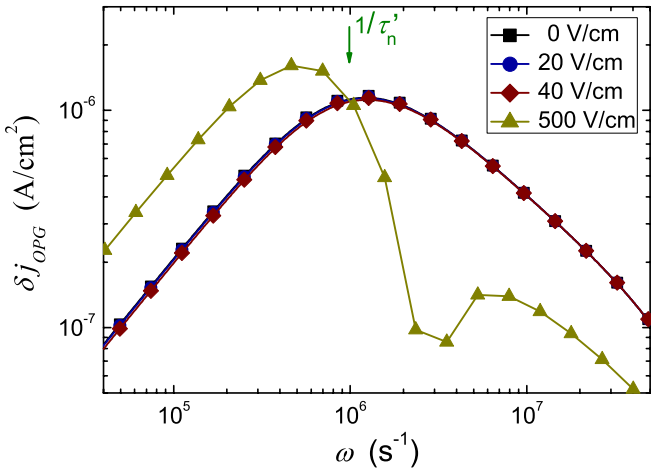


**Figure 12.** Simulated OPG current density ($\delta j_{\mathrm{OPG}}$) for different values of the external electric field indicated in the figure. In this simulation the grating period is $\Lambda = 40$ m and the generation rate is $G_0 = 10^{21}\,\mathrm{cm^{-3}\,s^{-1}}$.

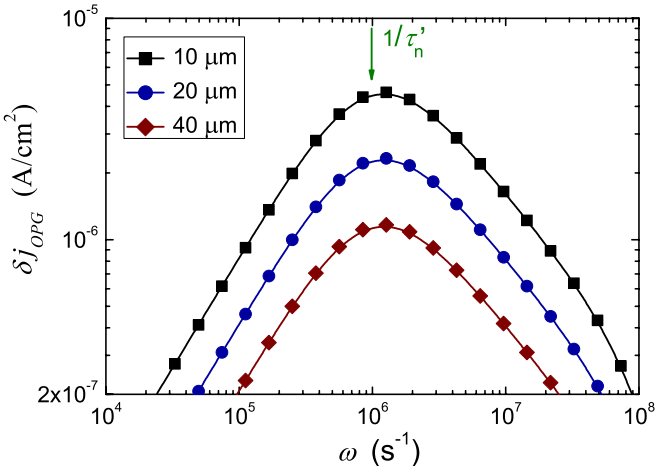


**Figure 13.** Simulated OPG current density ($\delta j_{\mathrm{OPG}}$) for different values of $\Lambda$ indicated in the figure. The generation rate here is $G_0 = 10^{21}\,\mathrm{cm^{-3}\,s^{-1}}$ and the external electric field is zero.

the quantitative agreement between figures 12 and 3 is not so good: the values of $\omega_{\max}$ and $\delta j_{\mathrm{OPG}}(\omega_{\max})$ differ. However, the qualitative agreement is excellent. Both in the experiment and in the calculations, these relatively small external fields produce no changes in the OPG signal and the curves are perfectly superimposed. This can be understood since a small electric field produces a vertical displacement of the curve shown in figure 2(*b*), without changing its shape. The lock-in amplifier used for the detection of the signal filters this constant value, giving an output value independent of the presence of a small external electric field. On the other hand, for high external electric fields the shape of the OPG curves changes completely, as can be seen in figure 12 for the case of $\xi_{\mathrm{ext}} = 500\,\mathrm{V\,cm^{-1}}$. This happens when $\xi_{\mathrm{ext}}$ is no longer negligible compared with $\xi_{\mathrm{int}}$, introducing an asymmetry in the grating movement. Although this is an interesting situation, we will not enter into details in this work.

The simulated outcome of varying the grating period is exhibited in figure 13. It is clear that the effect of decreasing $\Lambda$ is an increase in the photocurrent, while the peak of the curves is always located at the same angular frequency, in qualitative agreement with the measurements of figure 4. As already mentioned, the generation rate used in our measurements of figure 4 ($G_0 = 6.0 \times 10^{20}\,\mathrm{cm^{-3}\,s^{-1}}$) and in these simulations ($G_0 = 10^{21}\,\mathrm{cm^{-3}\,s^{-1}}$) locates the sample in the lifetime regime. As shown in figure 10, in this regime $\omega_{\max}$ is related to the inverse of the small signal lifetime, $\tau_n'$. Since a variation in the grating period does not change $\tau_n'$, which is fixed by the DOS and the generation rate, no shift in $\omega_{\max}$ is expected. On the other hand, a decrease in the grating period causes an intensification of the internal electric field due to the shorter separation between charges. This explains why the OPG signal increases with the decrease in $\Lambda$. The value of $\omega_{\max}$ in figure 4 is $\approx 2.5 \times 10^5\,\mathrm{s^{-1}}$ for all the curves, corresponding to a small signal lifetime $\tau_n' \approx 4\,\mu$s, a reasonable value for device-grade a-Si : H [21, 25].

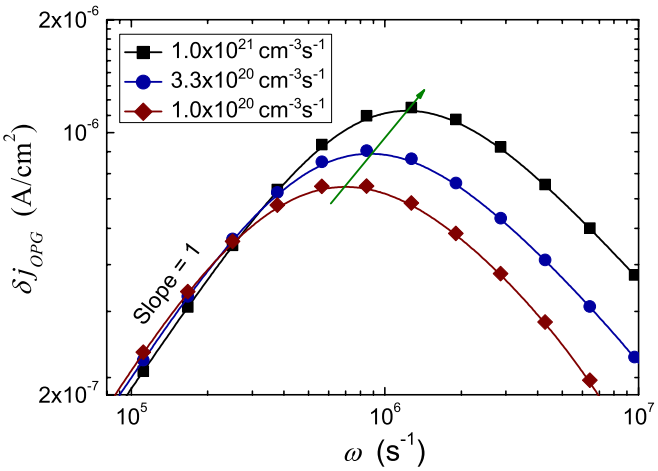


**Figure 14.** Simulation of the OPG current density ($\delta j_{\mathrm{OPG}}$) for different values of the generation rate indicated in the figure. The grating period is set to 40 $\mu$m and there is no external electric field.

Finally, figure 14 shows what happens when the generation rate is varied. In agreement with the measurements of figure 5, an increase in $G_0$ causes a shift of $\omega_{\max}$ towards higher values and an increase in the OPG current density. When the generation rate increases we have a decrease in $\tau_n'$ (figure 10), since the splitting of the quasi-Fermi levels turns more states into recombination centres, reducing the lifetime. Recalling the inverse relationship between $\omega_{\max}$ and $\tau_n'$ in the lifetime regime, the decrease in $\tau_n'$ results in an increase in $\omega_{\max}$. On the other hand, the increase in $G_0$ also increases the density of free carriers. This explains the increase in the maximum OPG signal with the generation rate seen in figures 5 and 14.

As can be seen by comparing figures 3–5 with figures 12–14, the trend of all the experimental results is well reproduced by the simulations. The goal of these simulations was not to perform a fit of the experimental results, but to gain some insight into the physical processes involved. The fact that a typical DOS for a-Si : H can reproduce the experimental trends is a cross-validation of our experimental and theoretical results.

### *5.4. Outline of DOS spectroscopy based on OPG measurements*

In addition to providing the dielectric relaxation lifetime and the small signal lifetime, the OPG experiment can also shed some light on the DOS of the material, as we shall show in the following. Indeed, the definition of the small signal lifetime leads to

$$\tau_n' = \frac{\partial n^{\mathrm{tot}}}{\partial G_0} = \frac{\partial n_0}{\partial G_0} + \frac{\partial n^{\mathrm{trap}}}{\partial G_0}. \tag{16}$$

Taking into account the power-law relationship between the free electron concentration and the generation rate, $n_0 \propto G_0^{\gamma}$, a straightforward calculation leads to

$$\frac{\partial n_0}{\partial G_0} = \frac{\gamma n_0}{G_0}. \tag{17}$$

On the other hand, we can write

$$\frac{\partial n^{\mathrm{trap}}}{\partial G_0} = \frac{\partial n^{\mathrm{trap}}}{\partial E_{\mathrm{F}n}} \frac{\partial E_{\mathrm{F}n}}{\partial n_0} \frac{\partial n_0}{\partial G_0}, \tag{18}$$

where $E_{\mathrm{F}n}$ is the electrons' quasi-Fermi level. The concentration of trapped electrons is given by

$$n^{\mathrm{trap}} = \int_{E_{\mathrm{v}}}^{E_{\mathrm{c}}} f_0(E) N^{\mathrm{ACC}}(E)\, \mathrm{d}E. \tag{19}$$

At low temperatures, the occupation function $f_0$ falls off sharply at $E_{\mathrm{F}n}$. If the temperature is such that $k_{\mathrm{B}}T$ (where $k_{\mathrm{B}}$ is Boltzmann's constant and $T$ the absolute temperature) is lower than the slope of the DOS between $E_{\mathrm{F}n}$ and $E_{\mathrm{c}}$, equation (19) can be approximated by

$$n^{\mathrm{trap}} \cong \int_{E_{\mathrm{v}}}^{E_{\mathrm{F}n}} f_0(E) N^{\mathrm{ACC}}(E)\, \mathrm{d}E. \tag{20}$$

Therefore, we have

$$\frac{\partial n^{\mathrm{trap}}}{\partial E_{\mathrm{F}n}} \cong f_0(E_{\mathrm{F}n}) N^{\mathrm{ACC}}(E_{\mathrm{F}n}). \tag{21}$$

From the definition of the electron quasi-Fermi level we have [26]

$$E_{\mathrm{F}n} = E_{\mathrm{c}} + k_{\mathrm{B}}T \ln\left[\frac{n_0}{N_{\mathrm{c}}}\right], \tag{22}$$

where $N_{\mathrm{c}}$ is the equivalent DOS at the conduction band edge. Therefore

$$\frac{\partial E_{\mathrm{F}n}}{\partial n_0} = \frac{k_{\mathrm{B}}T}{n_0}. \tag{23}$$

Substituting equations (21), (23) and (17) into (18), we obtain

$$\frac{\partial n^{\mathrm{trap}}}{\partial G_0} \cong \frac{k_{\mathrm{B}}T\gamma}{G_0} f_0(E_{\mathrm{F}n}) N^{\mathrm{ACC}}(E_{\mathrm{F}n}). \tag{24}$$

If we now substitute (17) and (24) into (16) we get

$$\tau_n' = \frac{\gamma}{G_0}[n_0 + k_{\mathrm{B}}T f_0(E_{\mathrm{F}n}) N^{\mathrm{ACC}}(E_{\mathrm{F}n})]. \tag{25}$$

For undoped a-Si : H samples at low temperatures we have $n_0 \ll k_{\mathrm{B}}T f_0(E_{\mathrm{F}n}) N^{\mathrm{ACC}}(E_{\mathrm{F}n})$ and, since electrons are the majority carriers, it can be demonstrated [26] that $f_0(E_{\mathrm{F}n}) \approx 1$. Thus

$$N^{\mathrm{ACC}}(E_{\mathrm{F}n}) \cong \frac{G_0 \tau_n'}{k_{\mathrm{B}}T\gamma}. \tag{26}$$

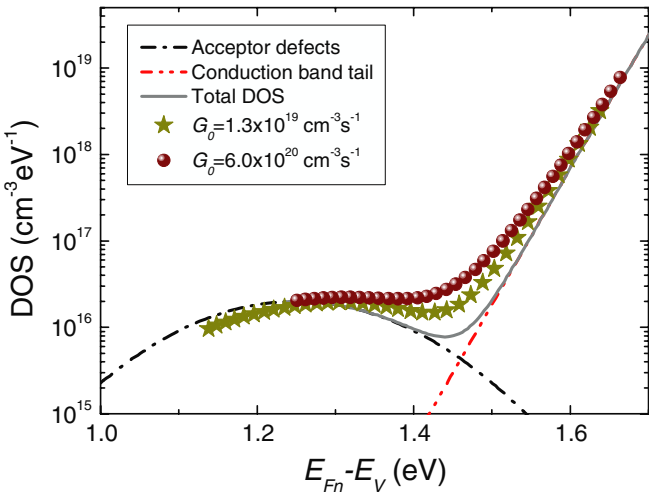


**Figure 15.** Simulations of a DOS spectroscopy based on the estimate of $\tau_n'$ combined with simple steady-state photoconductivity data. The simulation was performed at different temperatures from 100 to 460 K in steps of 10 K, with two different generation rates displayed in the inset.

Therefore, the knowledge of $\tau_n'$ from the OPG experiment, combined with very simple steady-state photoconductivity results, opens the possibility of achieving DOS spectroscopy. It is not the purpose of this paper to enter into a complete investigation on the possibilities and limitations of this DOS spectroscopy. Nevertheless, we shall illustrate the applicability of (26) by means of a numerical calculation. Introducing the DOS displayed in figure 6 into our computer code, we have performed calculations of $\tau_n'$ and $\gamma$ at different temperatures $T$, from 100 to 460 K in steps of 10 K, for two generation rates of $1.3 \times 10^{19}$ and $6 \times 10^{20}\,\mathrm{cm}^{-3}\,\mathrm{s}^{-1}$. Then we calculated the DOS according to equations (22) and (26), comparing with the originally introduced DOS. The final results are presented in figure 15 and one can see that the agreement between the introduced DOS and the calculated one is quite good. Although the slope of the conduction band tail is overestimated by ~20%, the general shape of the curve is well reproduced. We are at present working on the optimization of this DOS spectroscopy to improve the agreement between the 'true' DOS and the one deduced from OPG measurements.

Again, it was not the purpose of this paper to test all the possibilities offered by this new spectroscopy method. However, it is clear that the OPG method can provide information on important parameters of the sample, such as the dielectric relaxation time and the small signal lifetime, as well as on the DOS of the studied material when combined with simple steady-state photoconductivity measurements.

## 6. Conclusion

In this work we have presented the general equations describing the oscillating photocarrier grating technique and we have

clarified through numerical simulations the origin of the OPG signal. We have also implemented the experiment, applying it to an a-Si : H sample. The typical OPG curves present a peak for a characteristic frequency of oscillation of the grating, $\omega_{\max}$. Our experiments and simulations show that this peak is not affected by the presence of a small external electric field; it changes its height but not the position when the grating period is varied, and it changes both height and position when the generation rate is varied. The general agreement between experiments and simulations gives us confidence on our understanding of the technique. We could identify $\omega_{\max}^{-1}$ with a characteristic time of the sample, which is the small signal lifetime if the experiment is performed in the lifetime regime or the dielectric relaxation time if the experiment is performed in the relaxation regime. Therefore, the OPG method provides a simple and convenient way to extract important information on these times characterizing the response of the sample to an external perturbation. Moreover, we have shown that the density of states at the electrons' quasi-Fermi level can be obtained from measurements of steady-state photoconductivity and OPG performed in the lifetime regime.

## Appendix

Figure A1 shows beams $I_1$ and $I_2$ entering the sample from air. Both beams are polarized along the $y$-axis. The EOM introduces a phase shift $\phi$ on beam $I_2$ without changing its polarization or intensity (figure 1), so the electric field vector inside the sample can be written as

$$\vec{E}_2 = E_2 \cos[\Omega t + K_2' z + \phi]\hat{j},$$

where $\Omega$ is the angular frequency of the electromagnetic wave and $K_2'$ is the wavevector of beam $I_2$ inside the sample. Beam $I_1$ forms an angle $\delta$ with the normal outside the sample and an angle $\delta'$ inside the sample, which are related by refraction's law $n_{\text{air}} \sin\delta = n_{\text{sample}} \sin\delta'$. The electric field of beam $I_1$ inside the sample can be written as

$$\vec{E}_1 = E_1 \cos[\Omega t + K_1' \cos(\delta') z - K_1' \sin(\delta') x]\hat{j}.$$

The modules of both wavevectors are equal, thus $K_1 = K_2 = K$ and $K_1' = K_2' = K'$, while the values outside and inside the sample are related by $K/n_{\text{air}} = K'/n_{\text{sample}}$. Therefore, we have $K' \sin\delta' = K \sin\delta$. The resulting electric field inside the sample is

$$\vec{E} = \vec{E}_1 + \vec{E}_2 = E_1 \cos[\Omega t + K' \cos(\delta') z - K \sin(\delta) x]\hat{j} + E_2 \cos[\Omega t + K' z + \phi]\hat{j}.$$

The time-averaged modulus squared is

$$\langle|\vec{E}|^2\rangle = I(x,t) = I_1 + I_2 + 2\sqrt{I_1 I_2}\cos[K \sin(\delta) x + K'(1 - \cos\delta') z + \phi].$$

In the $x$ direction the grating has a spatial period $\Lambda = \lambda/\sin\delta$, while in the $z$ direction we have $\Lambda_z = \lambda/(n_{\text{sample}}(1 - \cos\delta'))$. For the conditions used in our experiments, this grating in the $z$ direction can be ignored since it has a period much larger than the sample thickness.

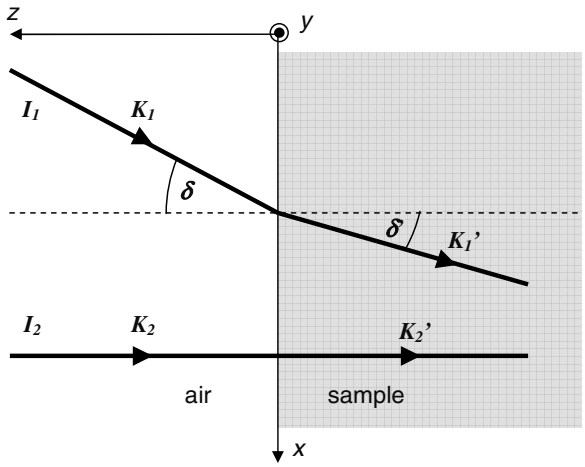


**Figure A1.** Schematic representation of the interfering beams going through the air–sample interface.

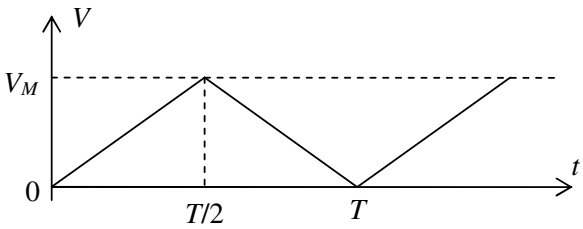


**Figure A2.** Voltage applied to the EOM as a function of time.

The modulated part of the illumination can thus be written as

$$\delta I(x,t) = 2\sqrt{I_1 I_2}\cos\left[\frac{2\pi}{\Lambda}x + \phi(V)\right],$$

where the voltage $V$ is the difference between the voltages applied to the two channels of the EOM. The resulting phase shift is linear with this voltage, so that

$$\phi(V) = \pi\frac{V}{V_{\text{M}}},$$

where $V_{\text{M}}$ is the maximum voltage that can be applied to the EOM, giving rise to a phase shift of $\pi$. To have a harmonic variation of the intensity with time we need a linear dependence of the angle $\phi$ with time, or a voltage applied to the EOM that is a triangular function with period $T$ (figure A2):

$$V(t) = \begin{cases} 2V_{\text{M}}\dfrac{t}{T} & \text{for} \quad 0 \leqslant t \leqslant \dfrac{T}{2}, \\ 2V_{\text{M}}\left(1 - \dfrac{t}{T}\right) & \text{for} \quad \dfrac{T}{2} \leqslant t \leqslant T, \end{cases}$$

$$\text{giving } \phi(t) = \begin{cases} 2\pi\dfrac{t}{T} & \text{for} \quad 0 \leqslant t \leqslant \dfrac{T}{2}, \\ 2\pi\left(1 - \dfrac{t}{T}\right) & \text{for} \quad \dfrac{T}{2} \leqslant t \leqslant T. \end{cases}$$

The result is

$$I(x,t) = I_1 + I_2 + 2\sqrt{I_1 I_2}\cos\left(\frac{2\pi x}{\Lambda} \pm \frac{2\pi t}{T}\right),$$

where the plus sign is for the first half of each period and the minus sign for the second half of each period. This is an intensity grating that periodically moves with a constant velocity in one direction for the first half of the period and in the other direction for the second half of the period. Defining $I_0 = I_1 + I_2$, $\delta I = 2\sqrt{I_1 I_2}$, $k = 2\pi/\Lambda$ and $\omega = 2\pi/T$ we finally have

$$I(x,t) = I_0 + \delta I \cos(kx \pm \omega t).$$

## Acknowledgments

This work was supported by MINCyT (Project 22-32515), CONICET (Project PIP 1464), UNL (Project CAI+D 68-349) and ECOS Sud-MINCyT (Project A08E01).

## References

[1] Ritter D, Zeldov E and Weiser K 1986 *Appl. Phys. Lett.* **49** 791
[2] Ritter D, Weiser K and Zeldov E 1987 *J. Appl. Phys.* **62** 4563
[3] Bauer G, Nebel C and Mohring H 1988 *Mater. Res. Soc. Symp. Proc.* **118** 679
[4] Yang L, Catalano A, Arya R and Balberg I 1990 *Appl. Phys. Lett.* **57** 908
[5] Goerlitzer M, Beck N, Torres P, Meier J, Wyrsch N and Shah A 1996 *J. Appl. Phys.* **80** 5111
[6] Badran R 2007 *J. Mater. Sci.: Mater. Electron.* **18** 405
[7] Duboz J, Binet F, Dolfi D, Laurent N, Scholz F, Off J, Sohmer A, Briot O and Gil B 1997 *Mater. Sci. Eng.* B **50** 289
[8] Schmidt J and Longeaud C 2005 *Phys. Rev.* B **71** 125208
[9] Haken U, Hundhausen M and Ley L 1993 *Appl. Phys. Lett.* **63** 3066
[10] Haken U, Hundhausen M and Ley L 1995 *Phys. Rev.* B **51** 10579
[11] Schmidt J, Hundhausen M and Ley L 2000 *Phys. Rev.* B **62** 13010
[12] Hattori K, Koji Y, Fukuda S, Ma W and Okamoto H 1993 *J. Appl. Phys.* **73** 3846
[13] Schmidt J, Budini N, Ventosinos F and Longeaud C 2010 *Phys. Status Solidi* a **207** 556
[14] Vinetskii V and Kukhtarev N 1975 *Sov. Phys.—Solid State* **16** 2414
[15] Trofimov G and Stepanov S 1986 *Sov. Phys.—Solid State* **28** 1559
[16] For a review see Stepanov S 2001 *Handbook of Advanced Electronic and Photonic Materials and Devices* vol 2 *Semiconductor Devices* ed H S Nalwa (London: Academic) p 205
[17] Petrov M, Sokolov I, Stepanov S and Trofimov G 1990 *J. Appl. Phys.* **68** 2216
[18] Trofimov G, Kosarev A, Kovrov A and LeComber P 1991 *J. Non-Cryst. Solids* **137&138** 483
[19] Kosarev A and Trofimov G 1994 *Int. J. Electron.* **76** 1023
[20] Abramov A, Kosarev A and Roca i Cabarrocas P 2000 *J. Non-Cryst. Solids* **266&269** 419
[21] Hattori K, Okamoto H and Hamakawa Y 1992 *Phys. Rev.* B **45** 1126
[22] Li Y 1990 *Phys. Rev.* B **42** 9025
[23] Antoniadis H and Schiff E 1991 *J. Non-Cryst. Solids* **137&138** 435
[24] Antoniadis H and Schiff E 1992 *Phys. Rev.* B **46** 9482
[25] Ritter D, Zeldov E and Weiser K 1988 *Phys. Rev.* B **38** 8296
[26] Longeaud C, Schmidt J and Kleider J 2006 *Phys. Rev.* B **73** 235316